Ocean Systems Engineering, *Vol. 13, No. 2 (2023) 195-224*
https://doi.org/10.12989/ose.2023.13.2.195

A study on development of simulation model of Underwater Acoustic Imaging (UAI) system with the inclusion of underwater propagation medium and stepped frequency beam-steering acoustic array

L.S. Praveen*[1], Govind R. Kadambi[1a], S. Malathi[1b] and Preetham Shankpal[2c]

[1]*Ramaiah University of Applied Sciences, Bangalore, India*
[2]*GE Health science, Bangalore, India*

(Received December 5 2022 Revised April 25, 2023, Accepted May 17, 2023)

Abstract. This paper proposes a method for the acoustic imaging wherein the traditional requirement of the relative movement between the transmitter and target is overcome. This is facilitated through the beamforming acoustic array in the transmitter, in which the target is illuminated by the array at various azimuth and elevation angles without the physical movement of the acoustic array. The concept of beam steering of the acoustic array facilitates the formation of the beam at desired angular positions of azimuth and elevation angles. This paper substantiates that the combination of illumination of the target from different azimuth and elevation angles with respect to the transmitter (through the beam steering of beam forming acoustic array) and the beam steering at multiple frequencies (through SF) results in enhanced reconstruction of images of the target in the underwater scenario. This paper also demonstrates the possibility of reconstruction of the image of a target in underwater without invoking the traditional algorithms of Digital Image Processing (DIP). This paper comprehensively and succinctly presents all the empirical formulae required for modelling the acoustic medium and the target to facilitate the reader with a comprehensive summary document incorporating the various parameters of multi-disciplinary nature.

Keywords: acoustic impedance; Inverse Synthetic Aperture Radar (ISAR); Inverse Synthetic Aperture SONAR (ISAS); Near-Field Beam Forming (NF-BF); Synthetic Aperture Radar (SAR); Synthetic Aperture SONAR (SAS); Underwater Acoustic Imaging (UAI); underwater environment

1. Introduction

Acoustics science is the study of sound and covers the study of the propagation of sound waves. Sound is one of the most efficient modes of communication in water because it can travel over long distances with low attenuation (considerably lower than the electromagnetic waves in water) (Christ *et al*. 2014). Sound waves also called Sound Navigation and Ranging (SONARs) are preferred for

*Corresponding author, Research Scholar, E-mail: lspraveen@msruas.ac.in
[a]Professor, E-mail: pvc.reserach@msruas.ac.in
[b]Professor, E-mail: malathi.ec.et@msruas.ac.in
[c]Data Architect, E-mail: preethshankpal@gmail.com

http://www.techno-press.org/?journal=ose&subpage=7 ISSN: 2093-6702 (Print), 2093-677X (Online)

exploring underwater applications. Water covers almost 71% of the earth's surface (Wang *et al.* 2012). Imaging an underwater scenario is an interesting but challenging problem. The acoustic imaging techniques are generally a result of traditional optical imaging and SONAR imaging techniques. As a qualified candidate for underwater applications, SONAR enables many practical applications such as detecting the submarine, mines, underwater communication, the study of the ocean's structure or biology, and the detection of archaeological artifacts.

One of the popular applications of underwater acoustic waves is Underwater Acoustic Imaging (UAI) which is a multi-disciplinary domain encompassing research in acoustic wave propagation, acoustic sensor beamforming and image processing among others. UAI helps in the generation of 2D images of underwater objects, which are important for distinguishing objects or studying their features. High-quality images of the targets/objects in underwater can be generated by the analysis of the acoustic wave propagation from the acoustic transducer elements of the transmitter unit through the underwater environment and back to the receiver elements. The underwater medium is considered one of the most difficult channels to model for imaging applications due to the high conductivity of water, strong presence of dissolved ion contents and penetration depth resulting in path loss (absorption loss + spreading loss), Propagation delay, and the ambient noise of acoustic waves in the medium (Shrivastava 2018). The medium through which the acoustic signals travel plays an important role since they undergo phenomena of reflection, attenuation, and path loss during the reconstruction of the image of the target. It is widely known that the depth of penetration of acoustic wave/signal through any medium decreases as the frequency of acoustic signal increases, but the resolution remains high. Acoustic waves undergo adiabatic compression and decompression resulting in the propagation of energy through a medium. Because of their vibration, acoustic waves are often considered as mechanical (González-García *et al*. 2020). When an acoustic wave travels through a medium, it produces local changes in the density of the medium as well as the displacement of mass.

It is suggested in (Melodia *et al.* 2013) that the propagation of sound in underwater is delayed and affected by the chemical and physical characteristics of water. Transmission loss occurs due to decreasing acoustic intensity when an acoustic pressure wave propagates in seawater. (Menna *et al.* 2016) discusses the development of a mathematical model for the acoustic medium of shallow water. The study illustrates the fundamental processes involved in the propagation of acoustic waves and certain simplifications for the developed model that allow critical parameters for underwater acoustic transducers. (Awan *et al.* 2019) illustrates that acoustic wave propagation in the underwater environment is a complicated phenomenon since many environmental variables influence it. Some of the factors affecting the wave propagation in underwater are propagation delays, noise by surroundings, path loss, attenuation, ambient noise, and multipath.

(Raihan *et al.* 2021) presents a method for the restoration of the underwater image to determine the depth. The method uses information on neutralized background light, blurriness, and red-light intensity. The transmission map is then computed using the determined depth, with different attenuation coefficients for direct and backscattered signals. The computed transmission map and background light are used to calculate the radiance of the scene. The performance of the proposed method was compared with the existing approaches using qualitative and quantitative analyses. However, this method has not addressed the images covering the entire range of underwater conditions which include different oceanic and coastal water types, and depth from different viewpoints. (Sung *et al.* 2020) discussed the technique to determine the yaw angle of the underwater target using a SONAR image. In this paper, a simulator for imaging an underwater target and an adversarial network to generate realistic template images of the target with shapes is presented. Later,

the yaw angle of the target is determined by comparing the template images with real SONAR images. The proposed technique is applicable for the localization of sources in underwater or multi-view-based underwater object recognition. However, the proposed method was tested in the indoor water tank with corresponding environmental parameters. Another method discussed in **(**Lee *et al.* 2020) is the detection of ships from images and videos using neural network-based object detection algorithms. The deep learning algorithm is used to detect static and floating objects such as speedboats, ships and buoys. However, the developed algorithm can detect objects on the surface of the water only but not under the water. Video frame information is not considered in the detection of the target.

It is widely known that the depth of penetration of acoustic waves through any medium decreases as the frequency of radiation increases, but the resolution remains high. The quality of images at lower frequencies is higher than the images obtained at higher frequencies. Stepped Frequency (SF) waveform leads to higher-quality images. It is achieved through the fusion of images from different frequency ranges (Ruliang *et al.* 2018). The SF SONAR imaging technique with low-range Side Lobe Peaks (SLP) was addressed by (Yang *et al.* 2018). To enhance the range resolution, the SF imaging method uses a pulse train in steps, which generates a large bandwidth. (Marx *et al.* 2000) presents a technique involving SF and Inverse Synthetic Aperture Radar (ISAR) processing to develop two-dimensional images of an aircraft target. The focus of the research in (Johnson *et al.* 2009) is on the effects of multipath contamination and resolution on image statistics. The analysis utilized the data from sea experiments, analytical and simulation modelling.

In Synthetic Aperture Radar (SAR) or in Synthetic Aperture SONAR (SAS), the target is stationary and the transmitter will be in motion. On the contrary, in ISAR or Inverse Synthetic Aperture SONAR (ISAS), the transmitter is stationary and the target will be in motion. Therefore, a relative motion between the transmitter and the target is a necessity for the formation of an image in SAR/SAS or ISAR/ISAS. One of the principal themes of this paper is to propose a method for acoustic imaging wherein the requirement of the relative motion between the transmitter and target is overcome. This is facilitated through the beamforming acoustic array in the transmitter, in which the target is illuminated by the array at various azimuth and elevation angles without the physical movement of the acoustic array. The concept of beam steering of the acoustic array facilitates the formation of the beam at desired angular positions of azimuth and elevation angles. In addition, the advantageous feature of SF in the formation of high-quality images is also incorporated in the developed simulation model of the UAI system. This paper substantiates that the combination of illumination of the target from different azimuth and elevation angles with respect to the transmitter (through the beam steering of beam forming acoustic array) and the beam steering at multiple frequencies (through SF) results in enhanced reconstruction of images of the target in the underwater scenario.

This paper also demonstrates the possibility of reconstruction of the image of a target in underwater without invoking the traditional algorithms of Digital Image Processing (DIP). Modelling of the medium of underwater propagation and the modelling of the target is essential in the development of a simulation model of the UAI system. This paper comprehensively and succinctly presents all the empirical formulae required for modelling the acoustic medium and the target to facilitate the reader with a comprehensive summary document incorporating the various parameters of multi-disciplinary nature. The modelling of underwater medium is carried out by considering acoustic characteristics such as propagation delay, path loss (spreading loss + absorption loss), noise, and material properties of seawater. This paper presents the nomograms of the acoustic medium by considering temperature, salinity, frequency, and pressure concerning depth to select an appropriate parameter for the UAI system.

The methodology of the paper's contribution is explained as follows:

Outcome 1: - Generic and versatile novel technique to determine near field radiation patterns of acoustic transducer element whose aperture can be any geometric configuration and simulate the same with beam steering feature to scan a 3D space

Task 1: Simulation of acoustic sensors in 2D array configurations for UAI

Task 2: Mathematical formulation and analysis of radiation pattern of acoustic array elements

Task 3: Simulation and analysis of array configuration with appropriate beam forming techniques

Task 4: Modelling of 3D space with scattering elements and scanning with developed beam steering technique

Task 5: Reconstruction of the 3D space using simulator

Outcome 2: - To model and simulate the underwater propagation medium

Taks 1: Modelling of underwater channel by incorporating the following parameters

- Wave propagation delay
- Path loss (Absorption Loss and Spreading loss)
- Noises (Ambient noise and Biological noise)
- Material property of seawater

Task 2: Modelling and simulation of beam steering in azimuth and elevation angles with the developed underwater channel

Outcome 3: - To simulate the stepped frequency waveform, integrate it to 2D beamforming array and evaluate the radiation pattern of 2D beamforming array for Underwater environment

Task 1: Simulation of stepped frequency waveforms for under water scenario

Task 2: Integration of the developed 2D beamforming array with stepped frequency waveform

Task 3: Simulation of 2D beamforming array with stepped frequency waveform for underwater scenario

Outcome 4: - To implement appropriate image reconstruction method needed for UAI System

Task 1: Development of an image reconstruction method for underwater scenario incorporating the following parameters:

- Target identification
- Lower clutter noise in images
- Lower computation time

Task 2: Validation of the developed image reconstruction method with target/object images captured underwater for their contour, shape and structure

Task 3: Testing and validating the developed UAI system in presence of various objects materials in underwater

A schematic representation of the placement of the transceiver (transmitter/receiver) and the target in seawater is shown in Fig. 1. It is pertinent to state that a single subsystem namely the transceiver performs the roles of both the Underwater Acoustic transmitter and the receiver. During the transmit mode of operation of the transceiver, the target is illuminated by the transmitter (Fig. 1(a)). The acoustic signal resulting after the reflection from the target (after its illumination) is received by the receiver of the same transceiver during the receive mode of operation. Fig. 1(b) depicts the two reflected signals from the target received during the receive mode of operation.

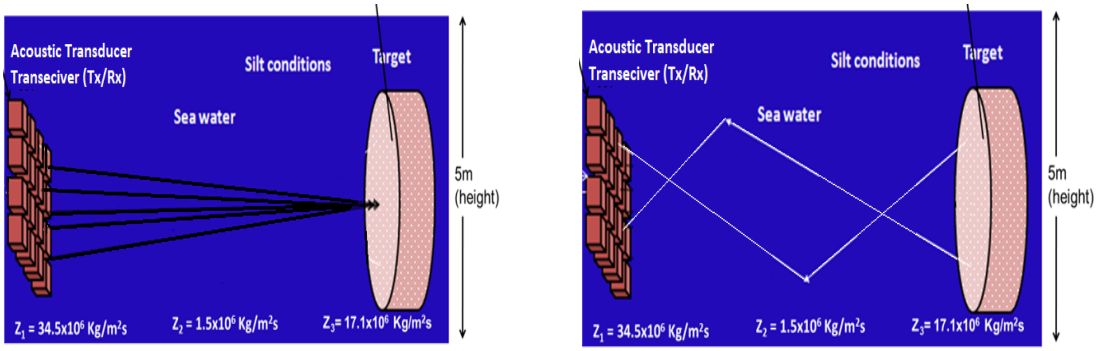

(a) Transmitter (b) Receiver

Fig. 1 Block Diagram of Underwater Acoustic Transceiver

This paper is organized through the following sections. Section 2 presents the modelling of underwater propagation medium for acoustic imaging; Section 3 deals with the physical properties of seawater; The nomograms of physical properties of seawater are presented in Section 4; Section 5 presents the transmission and reception of acoustic waves for UAI System in the underwater medium; Section 6 describes the stepped frequency waveform for UAI system; Section 7 presents the results and discussion of UAI system. The conclusions derived through analysis and simulation results of the UAI system model are presented in Section 8.

2. Modelling of underwater propagation medium for acoustic imaging

The acoustic imaging approaches are normally a result of traditional optical imaging, radar imaging, and SONAR imaging techniques. Technical advancements show that one can use energy outside the band of frequencies called light to detect and image the objects over very long distances. For example, radar uses radio waves, and the optical system uses cameras. Since the oceans are rather opaque to both light and radio waves, object detection using these methods is limited to very short distances. The strong presence of dissolved ion contents in seawater limits the penetration depth of light from a few centimetres to less than ten meters. To overcome this drawback, sound waves or acoustic waves or SONAR signals are used, which are not affected by the ion content or the higher densities of seawater. Hence, they are best suited for exploring the underwater environment. The acoustic waves are not affected by the depth since sound waves travel longer distances than light or radio waves in underwater. Regardless of this advantage, acoustic waves in underwater are affected by various environmental factors such as propagation delay, absorption loss, spreading loss, salinity, pressure, and frequency. In this section, the underwater environment factors affecting acoustic waves are discussed.

2.1 Propagation speed and delay

In water, the propagation speed of sound is faster than in air. The propagation speed of sound in air is around 343 meters per second under normal conditions, whereas the propagation speed of sound in water is around 1,480 meters per second. However, propagation speed of the sound is reduced when it is traveling from source to receiver due to underwater environment. Sound

propagation in underwater is delayed and affected by chemical and physical characteristics of water. The propagation delay varies with depth, transmission loss with frequency. The propagation delay increases even with a small change in depth. As the depth increases further, then there is only a slight change in propagation delay. The time it takes for a signal to travel from source to receiver called Propagation Delay (PD) is given by

$$PD = \frac{d}{c} \tag{1}$$

where,

d = distance between the transmitter and the receiver

c = Speed of sound

2.2 Transmission Loss (TL)

TL is the decrease in sound intensity between source and receiver. The TL depends on range and attenuation (Liu *et al.* 2017). Generally, TL will increase with the increase in frequency. The transmission loss is quantified through Eq. (2)

$$TL = 20 \times logr + \propto \text{ in dB} \tag{2}$$

where,

r = Range in meters

$\propto$ = Attenuation factor in dB given as:

$$\alpha = \frac{11e^{-5} \times f^2}{1+f^2} + \frac{44e^{-3} \times f^2}{4100+f^2} + 2.75e^{-7} \times f^2 + 3e^{-6} \tag{3}$$

f = Frequency in Hertz

2.3 Spreading Loss (SL)

Path loss occurs due to decreasing acoustic intensity when an acoustic pressure wave propagates in seawater. The path loss is divided into spreading loss and absorption loss. The major cause of acoustic signal attenuation in underwater is due to spreading and absorption loss. Spreading Loss is caused by the scattering of acoustic energy to the surface, leading to the expansion of acoustic waves. The path loss determines the loss of signal intensity after the commencement of wave propagation (wave transmission from the Transducer). In path loss, absorption loss increases with increasing range. However, the absorption coefficient increases with frequency at constant temperature and depth.

Spreading loss occurs when sound propagates through water from the source to the receiver. There are two types of spreading loss: cylindrical spreading and spherical spreading. The spherical spreading occurs more frequently than cylindrical spreading in seawater (Liu *et al.* 2017). The spreading loss is independent of frequency. However, it depends on distance and this loss increases as the distance between source and receiver increases. It is expressed by

$$SL(r) = k \times \log(r) \text{ in dB} \tag{4}$$

where,

r = Range in meter

k = 1 (cylindrical spreading) and k =2 (spherical spreading)

2.4 Absorption Loss (AL)

The absorption loss occurs in the form of heat resulting in energy loss. Due to viscous friction and ionic relaxation occurring in seawater, acoustic waves suffer absorption loss. This absorption loss increases with an increase in frequency (Liu *et al.* 2017). This absorption loss expressed by

$$AL = \alpha \times r \text{ in dB} \tag{5}$$

where,

r = range in meter

α = attenuation in dB expressed as:

$$\alpha = \frac{11e^{-5}\times f^2}{1+f^2} + \frac{44e^{-3}\times f^2}{4100+f^2} + 2.75e^{-7} \times f^2 + 3e^{-6} \tag{6}$$

2.5 Signal to Noise Ratio (SNR)

SNR is the signal strength related to background noise generated in underwater. Noise in underwater generally, decreases the signal strength during the propagation between the source and receiver. Noise in seawater is divided into two categories namely man-made noise and ambient noise. Man-made noise occurs due to ships, submarines, and AUVs, whereas ambient noise is caused by rain, wind, water movement and seawater creatures. Generally, ambient noise loss is up to 26 dB/km in seawater (Kularia *et al.* 2016). For shallow water, the SNR is more at lower frequency and decreases with increase in frequency. The SNR in dB is expressed as

$$SNR = SL - TL - NL + DI \tag{7}$$

where,

SL = Acoustic signal level in dB expressed as

$$SL = 169 + 10\log_{10}(P) - \alpha_s r - 20\log_{10}\left(\frac{d}{2}\right) - 10\log_{10}\left(r - \frac{d}{2}\right) \tag{8}$$

P = Radiated signal power in watts

α_s = Absorption co-efficient in dB/m

r =Range in m

d = Depth in m

TL = Transmission loss

NL = Noise level is 70 dB for Shallow water

DI = Acoustic Transducer Array Gain expressed as

$DI = 10\log\left(\frac{\pi D}{\lambda}\right)^2$ for Circular Aperture

$DI = 10\log\left(\frac{4\pi L_x L_y}{\lambda^2}\right)$ for Rectangular Aperture

3. Physical properties of seawater

Seawater has been formed over millions of years. Seawater covers the majority of the Earth's surface, around 71% of it. The physical, chemical and biological properties of the seawater are unique compared to water present on the land. It has several unusual properties in the distribution of temperature, pressure, salinity, pressure, velocity, and density due to its large volume and thickness. The quantity of heat and dissolved materials in the water affect the physical property of the water. The temperature is determined by the quantity of heat in the seawater. The salinity is determined by the quantity of dissolved matter and the pressure. The physical properties of seawater play a major role in underwater applications such as communication, imaging, and monitoring. The physical properties help to determine the acoustic impedance of seawater, objects in seawater, the velocity of sound, and density (Cruz 2011). Density is determined by using a mathematical function of salinity, temperature, and pressure. Acoustic impedance is determined by the density (ρ, in kg/m3) of the material and the speed of the sound waves (c, in m/s). Acoustic impedance helps to estimate the absorption and transmission loss of underwater material which also helps in the detection of underwater objects. Acoustic impedance is a measure of the resistance a sound wave encounters as it passes through a material. The bigger the difference in acoustic impedances between the two materials, the more is the reflection. No reflection occurs if two media/materials have the same acoustic impedance. To determine the acoustic impedance of seawater, it is required to know the physical property of seawater. This section presents some physical properties of seawater and its mathematical formulations.

3.1 Temperature

In seawater, temperature is one of the significant physical oceanographic variables. Temperature is a significant component in Earth's climate because it determines latent and sensible heat fluxes between the ocean and atmosphere. The water temperature is measured in degrees Celsius (^{o}C) and indicates the amount of energy spent or work done. The temperature of the seawater varies with depth, turbulence, geographic location, and heat generation. Solar radiation is reflected at the upper surface of the water, and it is absorbed with increasing in depth. It means that as one goes deeper in water, the resulting lesser sunshine leads to denser and heavier water than surface water. Temperature of sea water varies from -2℃ to +40℃, which is significantly lesser than the temperature of the air, which varies from -60℃ to +60℃. The temperature of the surface seawater varies a lot more than the temperature at the deep-water. It also varies with geographical locations and season. The temperature profile of seawater with respect to depth is addressed in (Saleha *et al.* 2021). The change in temperature of seawater affects the density. As the temperature decreases, the density of the seawater increases, which helps to determine the acoustic impedance of underwater materials.

3.2 Pressure

The pressure in the seawater is referred to as hydrostatic pressure. The pressure exerted on submerged objects by the weight of water is known as hydrostatic pressure. Pressure in seawater increases with an increase in depth. Unit for the pressure is pascal or bar or psi or atm or kg/cm^2. At the surface of seawater, pressure is at one atmosphere. Pressure increases linearly with depth. For every 10 m rise in-depth, pressure increases by 1 atm. Pressure Profile of seawater with respect to

depth is discussed in (Webb 2020). This leads to very high pressure in deep water compared to shallow water or the surface of the seawater. By considering the average depth of the sea on earth, the pressure is 381 times greater than the pressure at the surface of seawater. Pressure influences the density, biological and chemical properties of the seawater.

3.3 Salinity

The term "salinity" refers to the amount of "saltiness" in saltwater. The salinity of seawater is determined by the salts and ions content that dissolve in it. The number of grams of salt per kilogram in water is the measure of salinity which is expressed in Parts Per Thousand (PPT). The symbol for parts per thousand is ‰. The measure of electrical conductivity in seawater helps to determine the ionic content present in water which in turn helps to determine practical salinity value. This electrical conductivity of seawater is dependent on temperature and pressure. Hence it is also required to measure temperature and pressure to determine salinity value. The salinity value of seawater varies between $2 \leq S \leq 42$ PPT, but it can vary significantly in different locations. The average salinity of the oceans is 34.7 PPT, which means 34.7 g of salt per kilogram of saltwater. The salinity value in freshwater is less than in seawater. The variation of salinity affects the temperature and density of seawater. Salinity profile of seawater with respect to depth is presented in (Vigness-Rapose *et al*. 2012). The change in salinity value of seawater with depth depends on geographical location such as high and low latitudes. The salinity value changes slowly at the surface of the seawater. As the depth increases, salinity increases rapidly.

3.4 Density (ρ)

The "density is defined as mass per unit volume of a substance". The symbol of density is "ρ" and the unit for density is (kg/m^3). The density of seawater varies from 1020 to 1050 kg/m^3. The density of seawater depends on temperature, pressure, and salinity. The density of seawater is increased by decreasing its temperature, increasing its pressure, and salinity. However, pressure has the least impact on density because water is incompressible. Temperature and salinity play a major factor to determine density. Among these, temperature has the larger impact.

With the increase in depth, the density of seawater rapidly increases, called pycnocline (the region where there is a significant change in density). With further increase in depth, seawater temperature decreases, and salinity increases, leading to an increase in density known as thermocline (sudden change in temperature over depth) (Trujillo *et al.* 2014). Similarly, the density of seawater increases with an increase in pressure (Vigness-Rapose *et al*. 2012). As pressure increases, water molecules become tight resulting increase in weight of water. This leads to an increase in density.

The density (ρ, kg/m^3) of seawater is determined by the salinity of water (S, PPT), the temperature (t, ^{o}C) and the applied pressure with respect to depth (p, bars) using the formula of (Tenzer *et al.* 2011) and is given by Eq. (9)

$$\rho(S,t,p) = \frac{\rho(S,t,0)}{1-\frac{p}{K(S,t,p)}} \tag{9}$$

where, ρ(S, t, 0) is the normal atmospheric pressure of state of seawater (p=0) is given by

$$\rho(S,t,0) = \rho_{SMOW} + B_1 S + C_1 S^{1.5} + d_0 S^2 \tag{10}$$

Calculation of the Standard Mean Ocean Water (SMOW) density given by

$$\rho_{SMOW} = 999.842594 + 0.06793t - 0.009095290t^2 + 0.1001685 \times 10^{-3}t^3 - 0.0011200 \times 10^{-3}t^4 + 0.006536 \times 10^{-6}t^5 \quad (11)$$

$$S = 0.0080 - 0.1692K_t^{\frac{1}{2}} + 25.3851K_t + 14.0941K_t^{\frac{3}{2}} - 7.0261K_t^2 + 2.7081K_t^{\frac{5}{2}} \quad (12)$$

$$B_1 = 0.82449 - 0.0040899t + 0.076438 \times 10^{-3}t^2 - 0.8246 \times 10^{-6}t^3 + 0.005387 \times 10^{-6}t^4 \quad (13)$$

$$C_1 = -0.005724 + 102.27 \times 10^{-6}t - 1.654 \times 10^{-6}t^2 \quad (14)$$

$$d_0 = 0.00048314 \quad (15)$$

K(S, t, p) is the secant bulk modulus given by:

$$K(S,t,p) = K_1(S,t,0) + Ap + Bp^2 \quad (16)$$

where

$$K_1(S,t,0) = K_w + (54674.6 \times 10^{-3} - 603.459 \times 10^{-3}t + 0.0109t^2 - 61.67 \times 10^{-6}t^3)S + (0.07944 + 0.01648t - 0.00053t^2)S^{\frac{3}{2}} \quad (17)$$

$$A = A_w + (0.00228 - 10.981 \times 10^{-6}t - 1.607 \times 10^{-6}t^2)S + 0.1910 \times 10^{-3}S^{\frac{3}{2}} \quad (18)$$

$$B = B_w + (-0.9934 \times 10^{-6} + 20.816 \times 10^{-9}t + 0.9169 \times 10^{-9}t^2)S \quad (19)$$

For seawater the terms K_w , A_w *and* B_w of the secant bulk modulus are given by

$$K_w = 19.652 \times 10^3 + 0.14842 \times 10^3 t - 0.002327 \times 10^3 t^2 + 0.0136t^3 - 51.552 \times 10^{-56}t^4 \quad (20)$$

$$A_w = 3239.9 \times 10^{-3} + 1437.13 \times 10^{-6}t + 116.092 \times 10^{-6}t^2 - 0.5779 \times 10^{-6}t^3 \quad (21)$$

$$B_w = 0.08509 \times 10^{-3} - 0.006122 \times 10^{-3}t + 0.0527 \times 10^{-6}t^2 \quad (22)$$

The practical salinity varies from 0 to 42, temperature from -2 to 40°C and applied pressure from 0 to 1000 bars. To eliminate the effect of pressure on density, a quantity called $\sigma_{s,t,p}$ (called σ_t) is calculated by Eq. (23)

$$\sigma_{s,t,p} = (\rho(S,t,p) - 1) \times 1000 \quad (23)$$

3.5 Acoustic Impedance (Z)

Water is a good conductor of sound waves compared to air. The attenuation of sound waves in water is due to the absorption and conversion of sound into various forms of energy. It is a function of frequency of sound and water characteristics. The sound waves travel in water at a speed of 1500 m/s. The speed of sound in seawater is not constant, and it varies from season to season, place to place, morning to evening, and varies with depth. Although the variation is minimal, it plays an essential factor in the determination of acoustic impedance. The speed of the sound is affected by the physical property of seawater, such as temperature, pressure, and salinity. The speed of sound in seawater increases with increasing temperature, pressure, and salinity. Generally, density in freshwater is less compared to seawater. The density of seawater varies from 1020 to 1050 kg/m^3.

The density of seawater increases by decreasing temperature and by increasing pressure and salinity. The density of seawater is not measured directly. It can be measured using seawater's temperature, salinity, and pressure value. The density is determined by using Eq. (9). Acoustic impedance (Z) is determined by the density of seawater (ρ, kg/m^3) and the speed of the sound wave (c, m/s). Acoustic impedance is a measurement of the resistance to acoustic flow caused by acoustic pressure. It is generated at a given frequency by the vibrating of molecules in an acoustic medium. If the density and speed of sound increase, the acoustic impedance of seawater also increases. The acoustic impedance helps to differentiate the underwater materials, which in turn helps to explore the underwater environment. This is because the ability of a sound wave to pass from one medium/material to another is determined by the difference in acoustic impedance between the two medium/material types. If the sound is reflected, then the difference between the two mediums/material is more. The acoustic impedance is given by:

$$Z = \rho c \tag{24}$$

where, ρ is the density and c is the velocity of the sound in the material.

4. Nomograms of physical property of seawater

From the above discussion, it is evidently clear that seawater's physical properties play a vital role in the determination of acoustic impedance. The acoustic impedance of seawater is calculated by using the temperature, salinity, pressure, and density of seawater. The literature reveals that the physical properties of seawater will vary with geographical locations and varies with depth. To determine the value of acoustic impedance, it is required to select an appropriate value of temperature, pressure, salinity with respect to depth. This section presents the nomograms of the physical properties of seawater with respect to depth. The geographical location of the Bay of Bengal is selected to analyse temperature, salinity, and pressure to determine the acoustic impedance of underwater material. Fig. 2 shows the profile graph of acoustic impedance (Kg/m^{2}s) v/s depth (m) for the different physical properties of seawater, such as temperature, salinity, and pressure.

Fig. 2(a) shows the profile graph of acoustic impedance (Kg/m^{2}s) v/s depth (m) by keeping temperature (25^{o}C) and pressure (6.03 bar) constant and varying salinity. Fig. 2(b) shows the profile graph of acoustic impedance (Kg/m^{2}s) v/s depth (m) by keeping temperature (25^{o}C) and salinity (36.0 PPT) constant and varying pressure. Fig. 2(c) shows the profile graph of acoustic impedance (Kg/m^{2}s) v/s depth (m) by keeping temperature (25^{o}C) and pressure (6.03 bar) constant and varying salinity. Fig. 2 shows that the acoustic impedance will decrease with varying temperature, pressure, and salinity as the depth increases. For the UAI system analysis, to determine the acoustic impedance at fixed depth (10 m), salinity, temperature, and pressure values are selected using the graph shown in Fig. 2.

Further analysis of the physical property of seawater is carried out by a comparison of acoustic impedance v/s pressure, temperature, and salinity. Fig. 3(a) shows the acoustic impedance v/s pressure at constant temperature and varying salinity values. Fig. 3(b) shows the acoustic impedance v/s pressure by keeping salinity constant and varying temperature values. The results of Fig. 3 show that as the pressure increases, the acoustic impedance decreases.

Analysis of physical property of seawater is further carried out through the comparison of acoustic impedance v/s salinity by keeping temperature constant and varying pressure as illustrated

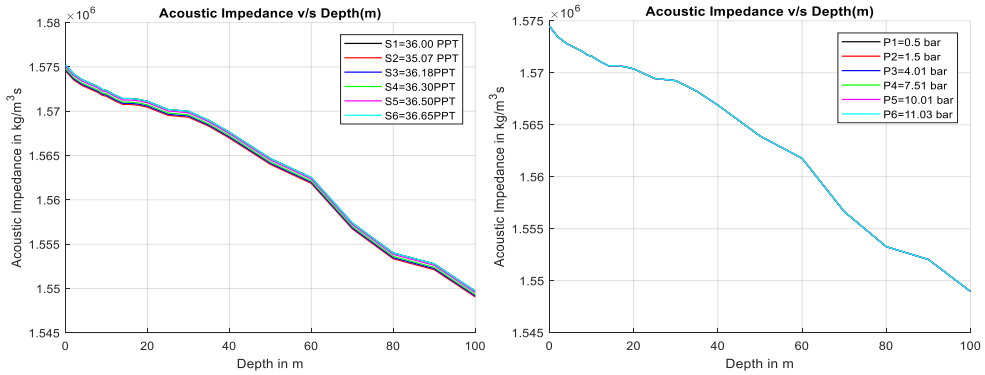

(a) T = 25.0°C & P = 6.03 bar (b) T = 25.0°C & S = 36.0 PPT

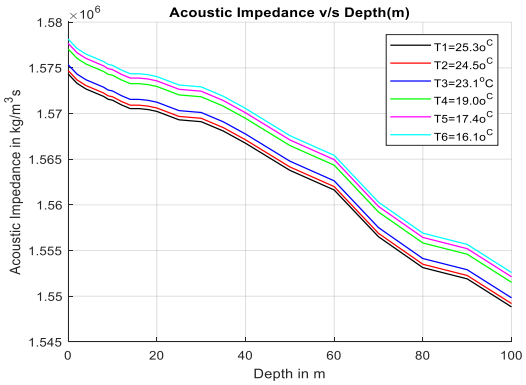

(c) P = 6.03 bar & S = 36.0 PPT

Fig. 2 Seawater profile of acoustic impedance vs depth

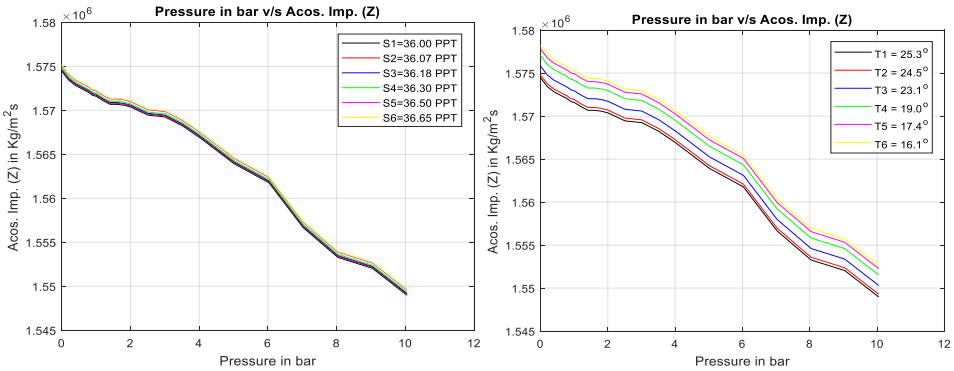

(a) T = 25.0°C (b) S = 36.0 PPT

Fig. 3 Seawater profile graph of acoustic impedance vs pressure

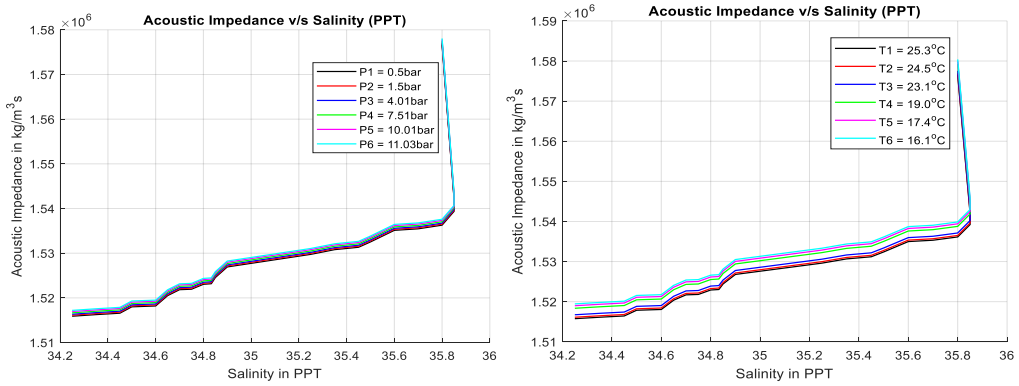

(a) T = 25.0ºC (b) S = 36.0 PPT

Fig. 4 Seawater profile graph of acoustic impedance vs Salinity

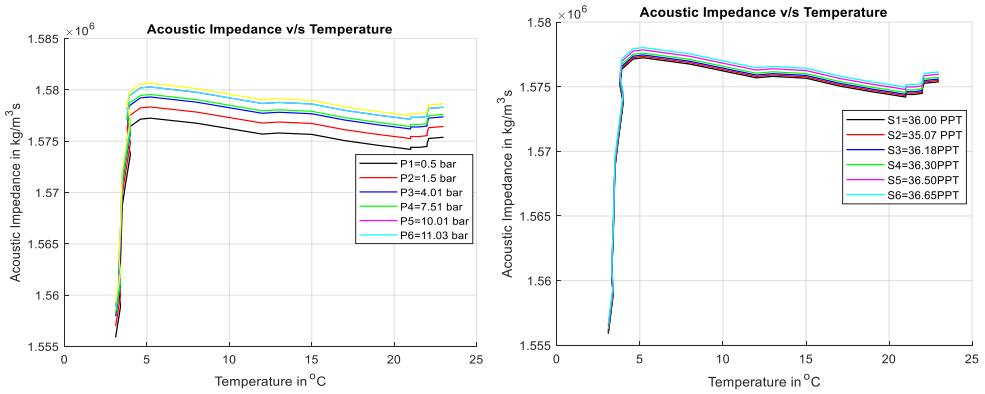

(a) S = 36.0 PPT (b) P = 6.03 bar

Fig. 5 Seawater profile graph of acoustic impedance vs temperature

in Fig. 4(a). Fig. 4(b) shows the acoustic impedance v/s salinity by keeping the pressure constant and varying the temperature. The results of Fig. 4 indicate that as salinity increases, the acoustic impedance decreases.

Analysis of physical property of seawater is also further carried out by comparing the acoustic impedance v/s temperature by keeping salinity constant and varying pressure value as illustrated in Fig. 5(a). Fig. 5(b) shows the acoustic impedance v/s temperature at constant pressure and varying salinity values. The results of Fig. 5 reveal that with the increase in temperature, the acoustic impedance decreases.

The acoustic impedance is calculated using Eq. (24) by the density of material or medium and velocity of sound. For the simulation results presented in this paper, we have considered the

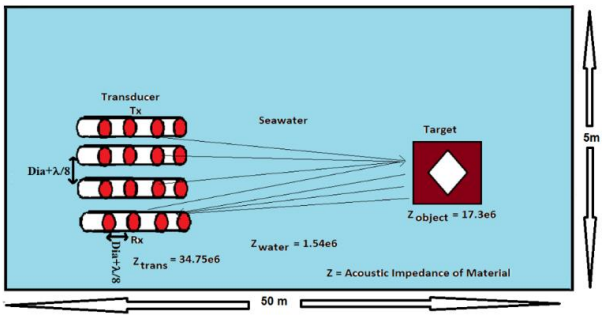

Fig. 6 Underwater propagation medium for UAI system

underwater acoustic paraments in the region of Bay of Bengal (Alam *et al.* 2022). In the region of Bay of Bengal, at of depth of 5 m, the salinity(S) is 35.85 PPT, temperature (T) is 21.5°C and pressure(P) is 0.5 bar. These values are well with in the range of salinity, temperature and pressure of regression Equations in (9)-(17) (Tenzer *et al.* 2011).

From Eq. (9) $\rho(S,T,P) = 1.0261 \times 10^3$

From Eq. (11) $\rho_{SMOW} = 997.982\ 09$

From Eq. (16) $K = 5.631 \times 10^4$

From Eq. (18) $A = 8.187 \times 10^4$

From Eq. (19) $B = -2.575 \times 10^{-5}$

From Eq. (20) $Kw = 2.186 \times 10^4$

From Eq. (9) $\rho(S,T,P) = 1.0251 \times 10^3$

5. Transmission and reception of UAI system

The modelled UAI system with the acoustic transducer as transmitter and receiver, modelled object/target and underwater medium is illustrated in Fig. 6. The novel approach for the computation of 2D radiation patterns of beamforming array with the array elements having a radiating aperture of either circular is discussed in Appendix. Using this approach, acoustic waves are transmitted from an acoustic transducer towards the target in the underwater environment. In the beamforming approach, the linear and planar array configurations are selected. For the UAI system, an underwater channel and pure conducting object are selected. For the simulation studies, the object was modelled as a flat metal plate with density ρ (kg/m³), the velocity of sound in water c (m/s), and acoustic impedance Z (Kg/m²s) for the underwater channel. For the simulation, 2D flat plate with different shapes such as a cross-shape, square-shape, horizontally strip vertical metal strip, circle, and plus shape are considered. In the simulation study, the acoustic impedance of acoustic transducer, seawater, and target are determined by using the information of density and speed of sound.

The amount of power transmitted or reflected at a boundary between three media/materials depends on the difference in acoustic impedance (Z) between the three. For the transmission coefficient in the UAI system, the acoustic impedance of the acoustic transducer is considered as "Z_1",

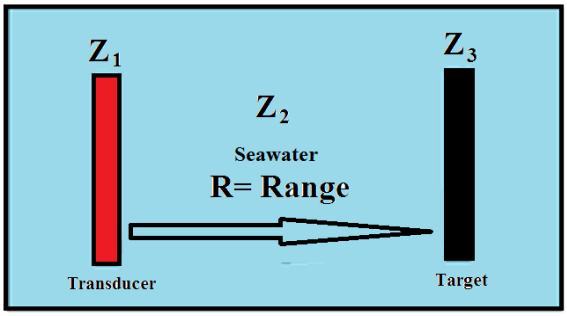

Fig. 7 Acoustic impedance of UAI system (Transmitter)

underwater environment as "Z_2" and target as "Z_3". The distance/range between transducer and target is "R" which is shown in Fig. 7. The expression for transmission co-efficient in UAI system is given by

$$T = \frac{4Z_1Z_2}{(Z_2+Z_1)^2cos^2kR+(Z_3+Z_1Z_2/Z_3)^2sin^2kR} \tag{25}$$

$$Tr_{co} = P^{NF}(R_{NF},\theta,\varphi,\theta_0,\varphi_0)|T|e^{-jLr} \tag{26}$$

where,

$P^{NF}(R_{NF},\theta,\varphi,\theta_0,\varphi_0)$ = Radiation pattern of beamforming array in near field region

L = PD+TL+SL+AL+SNR

r = R/cos(θ)

k = wave number (k = 2π/ λ, where λ is a wavelength)

R = Distance between transducer and target

$-90^0 \leq \theta \leq -90^0$

A pictorial representation of acoustic impedance of three media/material when acoustic signals are transmitted towards the target is shown in Fig. 7.

Similarly, during the reception cycle in the UAI system, the acoustic transducer is considered as "Z_3", the underwater environment as "Z_2" and target as "Z_1". The distance/range between transducer and target is "R" as shown in Fig. 8. The acoustic reflection co-efficient for UAI system is given as:

$$T = \frac{4Z_1Z_2}{(Z_2+Z_1)^2cos^2kR+(Z_3+Z_1Z_2/Z_3)^2sin^2kR} \tag{27}$$

$$Re = 1 - T \tag{28}$$

$$Re_{co} = Tr_{co} * |Re|e^{-jLr} \tag{29}$$

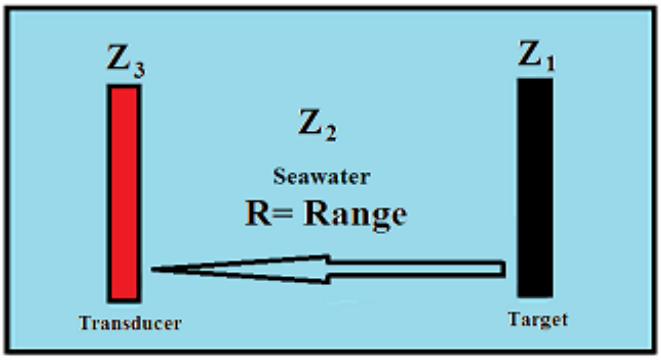

Fig. 8 Acoustic impedance of UAI system (receiver)

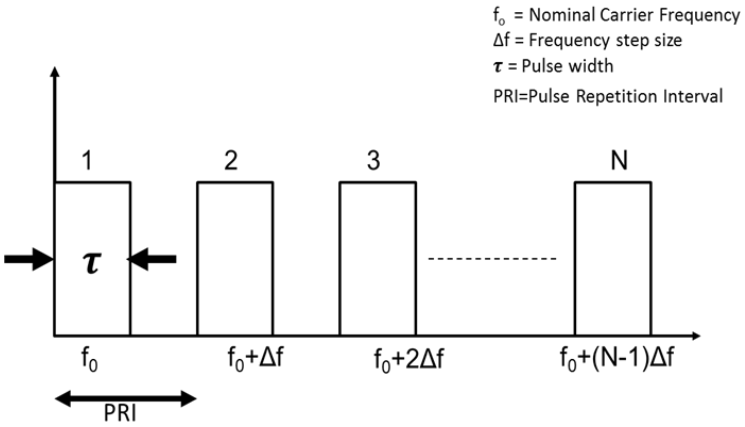

Fig. 9 Stepped Frequency Waveform

6. Stepped frequency waveform for UAI System

The proposed UAI system's main objective is to develop high-quality underwater images of the object by utilizing a stepped frequency waveform. It is widely known that the depth of penetration of radiation through any medium decreases as the frequency of radiation increases, but the resolution remains high. “It indicates that images taken at lower frequencies are of higher quality than images taken at higher frequencies. However, a stepped frequency waveform produces higher-quality images by fusing images from different frequency ranges” (Liu *et al.* 2017). The existing method such as intra-pulse compression, ultra-wideband and super-resolution techniques are used to obtained high range resolution. However, the main advantage of the stepped frequency waveform compared to the existing method is the use of wide bandwidth to obtain high range resolution. The requirement of narrow instantaneous bandwidth has less burden on A/D sampling requirements. The stepped frequency waveform is shown in Fig. 9. A sequence of N pulses is transmitted, with

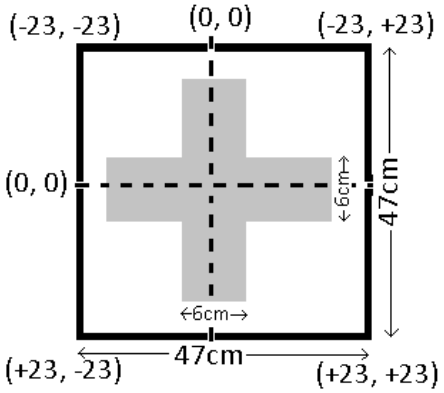

Fig. 10 The plus shape considered as target for UAI System

Table 1 Acoustic impedance of different materials

Material	**Density (ρ)(kg/m^3)**	**Speed of Sound (c)(m/s) In the medium/material**	**Acoustic impedance (Z) (Kg/m^{2}s)**
Aluminum	2690	6420	17.26x 10^6
Copper	11,090	3750	41.61 x 10^6
Stainless Steel	7860	5950	46.75 x 10^6
Iron	8873.04	5120	45.43 x 10^6
Glass	2709.2	4540	12.3 x 10^6
Medium(seawater)	1025.1	1480	1.5375 x 10^6

frequencies increasing in steps of Δf from pulse to pulse. The width of each pulse is given by τ. The frequency of the nth transmitted pulse is given by

$$f_n = f_0 + (n-1)\Delta f \qquad \text{n= 1, 2, 3,…,N} \qquad (30)$$

7. Results and discussion

The analysis and mathematical modelling of the underwater channel and stepped frequency waveform for the UAI system have been presented in the sections 2 to 6. With the help of this analysis, a simulation study is carried out for the proposed NF-BF presented in Appendix by considering the array elements having a radiating aperture of circular or rectangular contour. In the simulation, linear and planar array configurations are selected. The validation is carried out in both NF ($R_{NF} < 2D^2/\lambda$) and FF ($R_{FF} \geq 2D^2/\lambda$) region integrated with stepped frequency waveform in the underwater environment. In the simulation, the radius of the acoustic transducer of the circular aperture is considered as 2 cm. The length and width of the acoustic transducer with rectangular aperture are considered as (LxW) 3.14 x 4.00 cm. The number of elements considered for the simulation is N = 7, with an overall dimension of the linear array is 31.722 cm (adjacent gap chosen as λ/8) and a planar array of acoustic transducers with the elements (N=7x7) with an overall

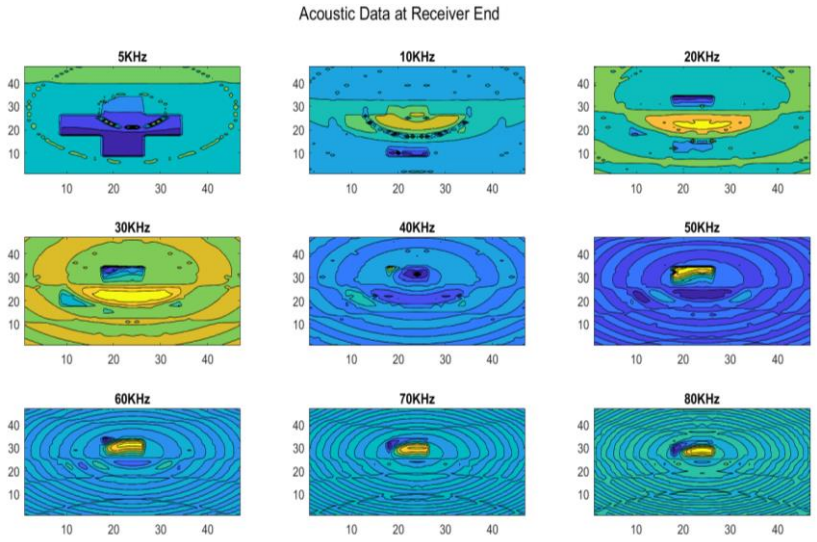

Fig. 11 Contour of reconstructed image of target at receiver end with stepped frequency (5 kHz to 80 kHz); linear array (N=7); array elements of circular aperture; $\theta_0 = 0^o$ & $\varphi_0 = 0^o$

dimension of the array is 31.722 cm (adjacent gap chosen as λ/8); the radius of circular aperture= 2 cm). Stepped frequency waveform is introduced to the simulation study by varying the frequency over a range of 5 kHz to 100 kHz in steps of 5 kHz. The target in underwater is illuminated by multiple scanning by varying beam steering angles in both the Azimuthal plane and Elevational plane. The 2D flat plate object is considered as the target (plus shape object illustrated in Fig. 10).

The dimensions of the target are 47 cm x 47 cm, and the thickness of the target is 1 cm. The underwater channel and object underwater are modelled with ρ, c, and z depending on the type of materials. Different materials with acoustic impedance (z) are tabulated in Table 1.

The results of contours of the reconstructed images of the target obtained through received data at the receiver acoustic transducer due to reflection from the target in the underwater environment are discussed in this section. Contour plots of reconstructed images are useful for many applications, including determining the location of any place or object and topographic mapping to show different levels of water or ground. Fig. 11 shows contour plots of the image of the target shown in Fig. 10 using the received acoustic signal obtained by the proposed NF-BF technique.

For the results shown in Fig. 11, the linear array elements (N=7) having a circular radiating aperture with a radius of 2 cm. The overall dimension of linear array configuration is 31.722 cm with an adjacent gap chosen as λ/8 is considered for NF-BF. The target is located in the underwater environment at near field region $R_{NF} = D^2/\lambda$ (203.69 cm). Beam steering (scan) is carried out at an angle $\theta_0 = 0^o$ and $\varphi_0 = 0^o$. For the simulation, Frequency of operation for both was varied from 5 kHz to 80 kHz. The chosen frequency is well within the SONAR operating frequency range of 1 kHz to 100 kHz. The simulation results illustrated in Fig. 11 indicate that at the lower frequency, the target's visibility is clear compared to that at higher frequency. As the frequency increases, the quality of the reconstructed image of the target degrades leading to a poor reconstruction of images because of increased loss of signal power at much higher frequencies.

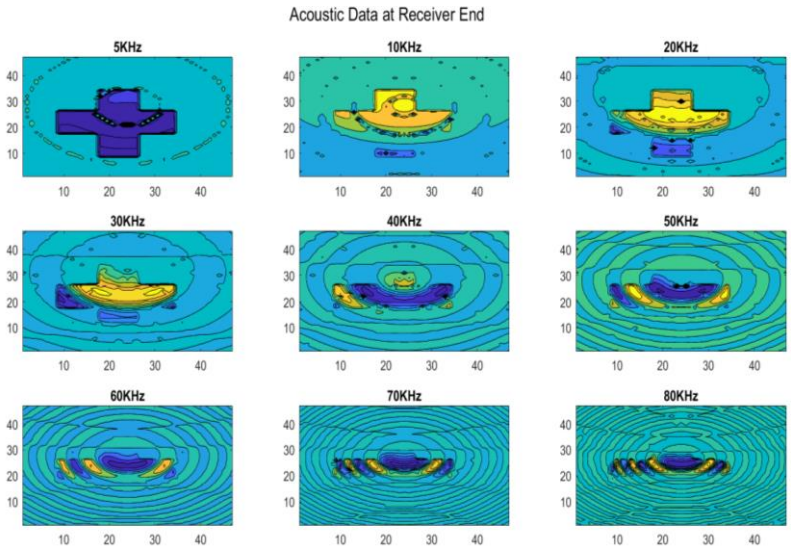

Fig. 12 Contour of reconstructed image of target at receiver end with stepped frequency (5 kHz to 80 kHz); linear array (N=7); array elements of circular aperture; $\theta_0 = 20^o$ & $\varphi_0 = 0^o$

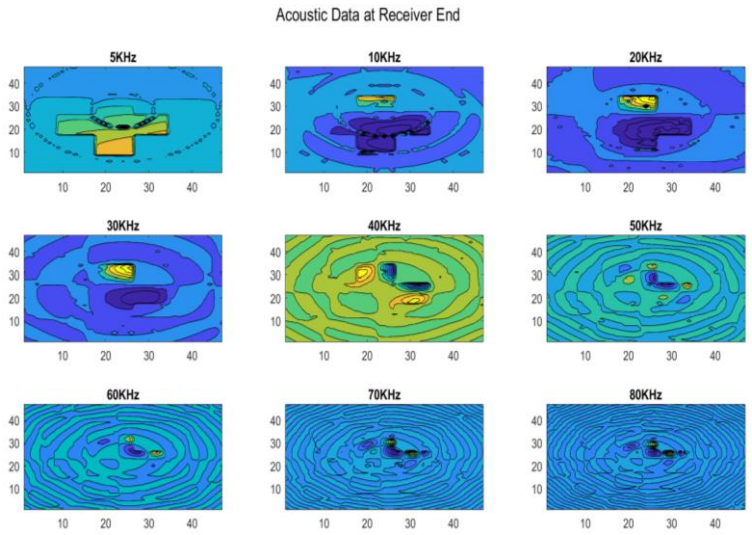

Fig. 13 Contour of reconstructed image of target at receiver end with stepped frequency (5 kHz to 80 kHz); planar array (N=7x7); array elements of circular aperture;$\theta_0 = 20^o$ & $\varphi_0 = 45^o$

Fig. 12 shows the contour plots of the image of the target shown in Fig. 10 using received acoustic signal data at near-field region $R_{NF} = D^2/\lambda$ (203.69 cm) by the beamforming linear array (N=7) with beam steering (scan) angle at $\theta_0 = 20^o$ and $\varphi_0 = 0^o$. In the simulation, stepped frequency is used, varying from 5 kHz to 80 kHz in the step of 10 kHz.

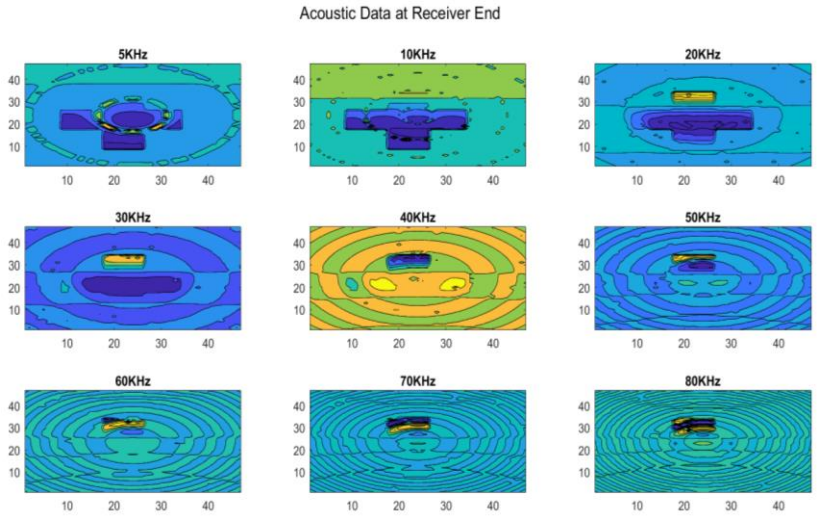

Fig. 14 Contour of reconstructed image of target object at receiver end with stepped frequency (5 kHz to 80 kHz); linear array (N=7); array elements of rectangular aperture; $\theta_0 = 20^o$ & $\varphi_0 = 0^o$

A further simulation study is carried out, replacing the linear array with a planar array configuration. For the proposed NF-BF technique, planar array configuration (N = 7x7) with the overall dimension of the planar array 31.722 cm with an adjacent gap chosen as λ/8 is considered. Fig. 13 shows the contour plot of the target image shown in Fig. 10 using an acoustic signal received by the beamforming planar array in near field region $R_{NF} = D^2/\lambda$ (203.69 cm) and beam steering (scan) angle at $\theta_0 = 20^o$ and $\varphi_0 = 45^o$. The simulation results shown in Fig. 13 indicate that there is a degradation in the quality of the reconstructed image at higher frequencies, leading to a poor reconstruction of images. The contour of the reconstructed image of the target does not correlate with the actual shape of the target.

The simulation study is also carried out for linear array configuration (N=7), with rectangular aperture instead of circular aperture. The dimensions of the acoustic transducer with rectangular aperture are (L x W) = (3.14 x 4.00) cm, and the overall dimension of linear array configuration is 31.726 cm with an adjacent gap chosen as λ/8. The scan (beam steering) angles used for the simulation are $\theta_0 = 20^o$ and $\varphi_0 = 0^o$. Fig. 14 shows the contour plot of the reconstructed image of the target shown in Fig. 10 using an acoustic signal received by the beamforming linear array in the near field region $R_{NF} = D^2/\lambda$ (203.69cm) and beam steering (scan) angle at $\theta_0 = 20^o$ and $\varphi_0 = 0^o$. In the simulation, stepped frequency is used to vary the frequency from 5 kHz to 80 kHz in the step of 10 kHz. The simulation results shown in Fig. 14 indicate that as the frequency increases, the quality of reconstruction of image degrades, eventually leading to a poor reconstruction of images. At higher frequencies, the contour of the reconstructed image of the target does not reflect the actual shape of the target/object.

The simulation study is also carried out using a planar array configuration instead of a linear array with array elements of rectangular aperture. For the proposed NF-BF technique planar array configuration (N = 7x7) with the overall dimension of the planar array, the configuration is 31.722 cm with an adjacent gap chosen as λ/8 is considered. Fig. 15 shows the contour plot of the

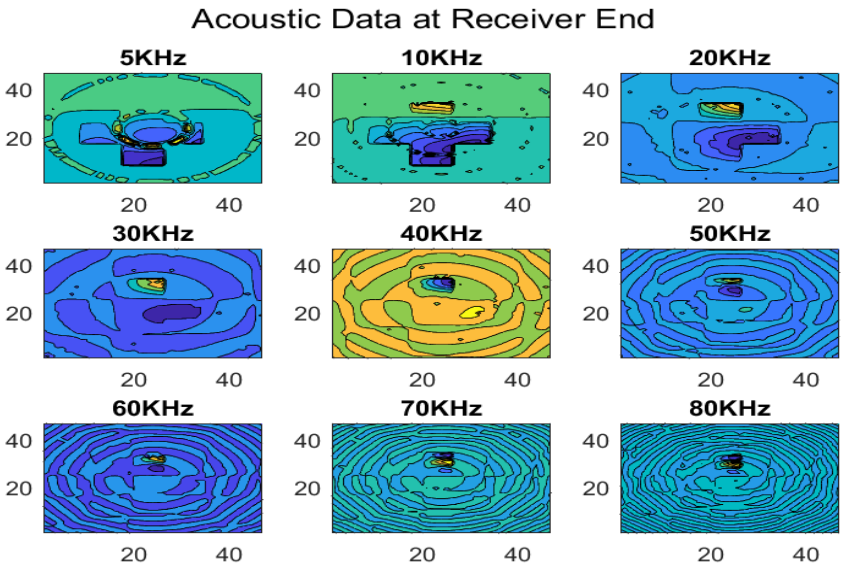

Fig. 15 Contour of reconstructed image of target object at receiver end with stepped frequency (5 kHz to 80 kHz); planar array (N=7x7); array elements of rectangular aperture; $\theta_0 = 20^o$ & $\varphi_0 = 45^o$

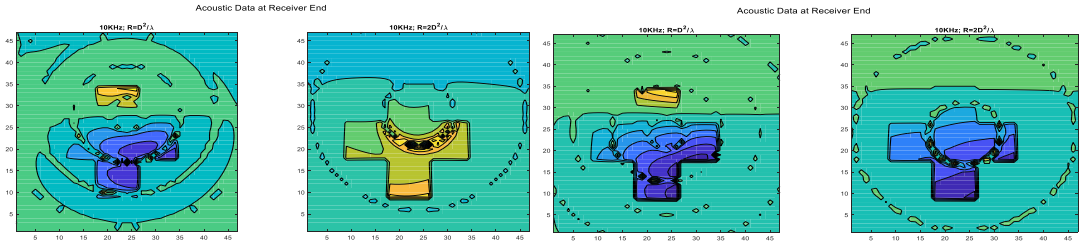

(a) $R_{NF} = D^2/\lambda$ (b) $R_{FF} = 2D^2/\lambda$ (c) $R_{NF} = D^2/\lambda$ (d) $R_{FF} = 2D^2/\lambda$

Fig. 16 Contour of reconstructed image of target at receiver end using linear array (N=7); $\theta_0 = 20^o$;$\varphi_0 = 0^o$

reconstructed image of the target shown in Fig. 10 using data of acoustic signal received by the beamforming planar array in the near field region $R_{NF} = D^2/\lambda$ (203.69 cm) and beam steering (scan) angle at $\theta_0 = 20^o$ and $\varphi_0 = 45^o$. In the simulation, stepped frequency is used to vary the frequency from 5 kHz to 80 kHz in the step of 10 kHz. The simulation results shown in Fig. 15 indicate that as the frequency increases, the quality of the reconstruction of the target image degrades.

Further validation of the proposed NF-BF technique in the underwater channel is carried out by comparing the reconstructed images carried out by the beamforming array placed in near-field and far-field regions. For the near-field region simulation, the distance between radiating array and target is at a distance $R_{NF} = D^2/\lambda$ (203.69 cm), and for the far-field region, the distance between radiating array and target is at a distance $R_{NF} = 2D^2/\lambda$ (407.38 cm). The overall dimension of the linear array (N=7) configuration is 31.722 cm with an adjacent gap chosen as $\lambda/8$. Fig. 16 shows the contour plot

of the reconstructed image of the target shown in Fig. 10 using an acoustic signal received by the beamforming acoustic array located in the near field with an operating frequency at frequency of 10 kHz.

Figs. 16(a) and 16(b) show the contour plot of the reconstructed image of the target using linear array configuration (N = 7) whose array elements have circular aperture with beam steering (scan) angle at $\theta_0 = 20^o$ and $\varphi_0 = 0^o$. The contour plot of the reconstructed image of the target shown in Fig. 16(a) is obtained at a near-field region $R_{NF} = D^2/\lambda$ (203.69 cm) from a beamforming linear array. Similarly, the contour plot image of the target shown in Fig. 16(b) is obtained at a far-field region $R_{FF} = 2D^2/\lambda$ (407.38 cm) from the acoustic beamforming array.

Figs. 16(c) and 16(d) show the contour plots of the reconstruction of the image of the target using the linear array (N=7) having array elements of rectangular aperture with beam steering (scan) angle at $\theta_0 = 20^o$ and $\varphi_0 = 0^o$. The contour plots reconstructed image of the target shown in Fig. 16(c) are obtained at a near-field region $R_{NF} = D^2/\lambda$ (203.69 cm). Similarly, the contour plots of the reconstructed image of the target shown in Fig. 16 (d) are obtained at a far-field region $R_{FF} = 2D^2/\lambda$ (407.38 cm). The results of Fig. 16 show that the reconstructed image of the target is distinctly visible in both near-field ($R_{NF} = D^2/\lambda$) and far-field regions ($R_{FF} = 2D^2/\lambda$) in the underwater environment. Hence, the proposed NF-BF technique is applicable for near-field and far-field regions in an underwater environment scenario.

The simulation results demonstrate that the reconstructed image at beam steering angles ($\theta_0 = 20^o$; $\varphi_0 = 45^o$) for both circular and rectangular aperture produce improved detection of target compared to reconstructed image of target at beam steering angle ($\theta_0 = 0^o$; $\varphi_0 = 0^o$). The simulation results illustrated in this section can be improved further by using image processing algorithms such as to detect the underwater target by removing noise and other disturbances. Some of the common image processing methods used to reconstruct the image of an object in underwater are back projection, fast factorized back-projection, explicit matched filtering algorithm, range migration (ω-k) algorithm, fuzzy logic fusion, PCA fusion and Multi-Resolution Analysis Based Method (Wang *et al.* 2015) among other techniques. The proposed simulation model presented in the paper is implemented with MATLAB software. The details of the computing machine used to obtain the results of the simulation model are:

- Operating system: Windows 10
- Processor: AMD Ryzen™ 5 5625U Processor (2.30 GHz upto 4.30 GHz)
- Memory: 8 GB Soldered DDR4 3200MHzClockspeed 2.4 Ghz
- Hard Drive: 512 GB M.2 2242 SSD PCIe Gen4/4
- Graphics: Integrated AMD Radeon™ Graphics

The software requirement and time used for this simulation model are given below:

MATLAB 2017a software tool is used for the implementation of proposed simulation model. For this tool the minimum system requirements are:

- Operating System: Windows 7 Service Pack 1
- Processor: Minimum: Any Intel or AMD x86–64 processor
- Memory: Minimum: 2 GB RAM
- Hard Drive: 2 GB for MATLAB only, 4–6 GB for a typical installation
- Graphics: No specific graphics card is required.

The execution time for the simulation model to obtain the reconstructed of the target is 40 sec.

8. Conclusions

This paper has presented mathematical modelling of the underwater channel for the UAI system. The underwater parameters such as propagation delay, path loss, and noise are considered in the modelling of the underwater medium. The mathematical formulations for underwater parameters used to determine the propagation loss of acoustic waves in an underwater medium are presented. To differentiate the influence of the choice of a medium and the material properties on the propagation of underwater acoustic waves, the acoustic impedance is determined by using the physical properties of seawater. The physical properties of seawater, such as temperature, salinity, pressure, and density, are used to determine the acoustic impedance for the acoustic transducer, seawater, and target object. Numerous simulation studies have demonstrated the feasibility of the NF-BF technique for the detection of the target in underwater using various frequencies of SONAR. The simulation results reveal that lower frequencies facilitate image reconstruction of good quality compared to higher frequencies.

The method proposed in this paper for acoustic imaging overcomes the traditional requirement of the relative movement between the transmitter and the target. The beamforming acoustic array in the transmitter facilitates the illumination of the target at various azimuth and elevation angles without the physical movement of the acoustic array. The concept of beam steering of the acoustic array facilitates the formation of the beam at desired angular positions of azimuth and elevation angles. This paper demonstrates that the combination of illumination of the target from different azimuth and elevation angles with respect to the transmitter (through the beam steering of beam forming acoustic array) and the beam steering at multiple frequencies (through SF) results in enhanced reconstruction of images of the target in the underwater scenario. This paper also illustrates the possibility of reconstruction of the image of a target in underwater without invoking the traditional algorithms of Digital Image Processing (DIP). Yet another contribution of this paper is the comprehensive and succinct presentation of all the empirical formulae required for modelling the acoustic medium and the target to facilitate the reader with a comprehensive summary document incorporating the various parameters of multi-disciplinary nature.

References

Al-Zhrani, S., Bedaiwi, N.M., El-Ramley, I.F., Barasheed, A.Z., Abduldaiem, A., Al-Hadeethi1, Y. and Umar, A. (2021), "Underwater optical communications: A brief overview and recent developments", *Engineered Sci.*, **16**, 146-186. https://doi.org/10.30919/es8d574.

Awan, K.M., Shah, P.A., Iqbal, K., Gillani, S., Ahmad, W. and Nam, Y. (2019), "Underwater wireless sensor networks: A review of recent issues and challenges", *J. Wireless Commun. Mobile Comput.*, 2-21. https://doi.org/10.1155/2019/ 6470359.

Basagni, S., Conti, M., Giordano, S. and Stojmenovic, I. (2013), *Mobile Ad Hoc Networking: Cutting Edge Directions*, Second Ed., The Institute of Electrical and Electronics Engineers, Inc.

Christ, R.D. and Wernli, R.L. (2014), *The ROV Manual-The Ocean Environment*, Butterworth-Heinemann Elsevier Ltd., 21-52. https://doi.org/10.1016/B978-0-08-098288-5.00002-6.

Cruz, N. (2011), "Autonomous underwater vehicles", Intech open, 113-173.

González-García, J., Gómez-Espinosa, A., Cuan-Urquizo, E., García-Valdovinos, L.G., Salgado-Jiménez, T. and Cabello, J.A.E. (2020), "Autonomous underwater vehicles: localization, navigation, and communication for collaborative missions", *Appl. Sci.*, **10**(4), 1256, https://doi.org/10.3390/app10041256.

Jarina Raihan A., Emeroylariffion Abas, P.G. and De Silva, L.C. (2021), "Restoration of underwater images using depth and transmission map estimation, with attenuation priors", *Ocean Syst. Eng.*, **11**(4), 331-351. https://doi.org/10.12989/ose.2021.11.4.331.

Johnson, S.F. (2009), "Synthetic aperture sonar image statistics", PhD Thesis, The Pennsylvania State University.

Kularia, Y., Kohli, S. and Bhattacharya, P.P. (2016), "Analyzing propagation delay, transmission loss and signal to noise ratio in acoustic channel for underwater wireless sensor networks", *Proceedings of the IEEE 1st International Conference on Power Electronics, Intelligent Control and Energy Systems (ICPEICES)*, 1-5. https://doi.org/10.1109/ICPEICES.2016.7853300.

Lee, S.J., Roh, M.I. and Oh, M.J. (2020), "Image-based ship detection using deep learning", *Ocean Syst. Eng.*, **10**(4), 415-434. https://doi.org/10.12989/ose. 2020.10.4.415.

Liu, X., Sun, C., Yang, Y. and Zhuo, J. (2017), "Low sidelobe range profile synthesis for sonar imaging using stepped-frequency pulses", *IEEE Geosci. Remote Sens. Lett.*, **14**(2), 218-221. https://doi.org/10.1109/LGRS.2016.2635154.

Marx, D., Nelson, M., Chang, E., Gillespie, W., Putney, A. and Warman, K. (2000), "An introduction to synthetic aperture sonar", *Proceedings of the 10th IEEE Workshop on Statistical Signal and Array Processing (Cat. No.00TH8496)*, 717-721. https://doi.org/10.1109/SSAP.2000. 870220.

Massel, S.R. (2015), *Internal gravity waves in the shallow seas*, Springer International Publishing Switzerland

Masud-Ul-Alam, M., Khan, M.A.I., Barrett, B.S. and Rivero-Calle, S. (2022), "Surface temperature and salinity in the northern Bay of Bengal: in situ measurements compared with satellite observations and model output", *J. Appl. Remote Sens.*, **16**(1), 018502-1-018502-19. https://doi.org/10.1117/1.JRS.16.018502.

Menna, B.V., Acosta, G.G. and Villar, S.A. (2016), "Underwater acoustic channel model for shallow waters", *Proceedings of the 23rd IEEE/OES South American International Symposium on Oceanic Engineering (SAISOE)*, 1-7, https://doi.org/10.1109/SAISOE.2016.7922471.

Praveen, L.S., Kadambi, G.R., Malathi, S. and Shankapal, P. (2020), "Computation of near-field and far-field radiation characteristics of acoustic transducers for underwater acoustic imaging", *Int. J. Commun. Antenna Propagation*, **10**(3), 145-150.

Praveen, L.S., Kadambi, G.R., Malathi, S. and Shankapal, P. (2021), "A generic approach for computation of near-field and far-field pattern of beamforming acoustic transducer array", *Int. J. Commun. Antenna Propagation*, **11**(6), 414-439.

Shrivastava, A. (2018), *Introduction to Plastics Engineering*, William Andrew Elsevier Ltd., 49-110 https://doi.org/10.1016/C2011-0-07796-7.

Sung, M. and Yu, S.C. (2020), "Sonar-based yaw estimation of target object using shape prediction on viewing angle variation with neural network", *Ocean Syst. Eng.*, **10**(4), 435-449. https://doi.org/10.12989/ose.2020.10.4.435.

Tenzer, R., Novák, P. and Gladkikh, V. (2011), "On the accuracy of the bathymetry-generated gravitational field quantities for a depth-dependent seawater density distribution", *Studia Geophysica et Geodaetica*, **55**, 609-626.

Trujillo, A. and Thurman, H. (2014), *Essentials of Oceanography*, United Kingdom: Pearson Prentice Hall.

Vigness-Raposa, K.J., Scowcroft, G., Miller, J.H. and Ketten, D. (2012), "Discovery of sound in the sea: An online resource", (Eds., Popper, A.N. and Hawkins, A.), *The Effects of Noise on Aquatic Life. Advances in Experimental Medicine and Biology*, **730**, Springer, New York, NY. https://doi.org/10.1007/978-1-4419-7311-5_30.

Wang, X., Zhang, X. and Zhu, S. (2015), "Upsampling based back projection imaging algorithm for multi-receiver synthetic aperture Sonar", *Proceedings of the International Industrial Informatics and Computer Engineering Conference*, 1610-1615.

Wang, Y., Liu, Y. and Guo, Z. (2012), "Three-dimensional ocean sensor networks: A survey", *J. Ocean*, Univ. China, **11**, 436-450. https://doi.org/10.1007/s11802-012-2111-7.

Webb, P. (2020), *Introduction to Oceanography*, In: University, R.W. (Ed.) Open Publishing. United States: Creative Commons Attribution 4.0 International License.

Yang, L., Zhou, S., Zhao, L. and Xing, M. (2018), "Coherent auto-calibration of APE and NsRCM under fast back-projection image formation for airborne SAR imaging in highly-squint angle", *Remote Sens.*, **10**, 321. https://doi.org/10.3390/rs10020321.

Yang, R., Li, H., Li, S., Zhang, P., Tan, L., Gao, X. and Kang, X. (2018), "Stepped-frequency waveform and SAR imaging in: High-resolution microwave imaging", *Springer Singapore*, 119-159.

RS

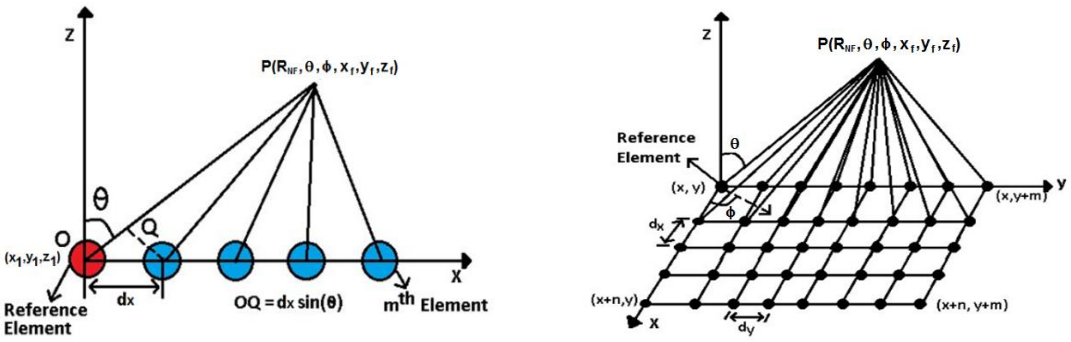

(a) Linear Array (b) Planar Array

Fig. A.1 Near-field beamforming linear array configuration (Praveen *et al.* 2020)

Appendix

This appendix presents a mathematical formulation of NF-BF array of acoustic transducers which is valid for both near-field and far-field regions. The mathematical formulation of NF-BF array of acoustic transducers which is valid for both near-field and far-field regions is presented in this appendix.

The concept of beamforming in near-field region for linear as well as planar array is illustrated in Fig. A.1(a) and Fig. A.1(b) respectively. Acoustic rays incident on (or) radiated from acoustic transducer elements are not parallel in near field. The distance between point of observation and individual transducer elements in the array cannot be assumed to be the same in NF-BF. Hence the spherical polar angles θ and φ subtended by the individual elements at the observation point are different.

The near field radiation pattern of the beamforming array at an observation point located in either far-field or near-field region with its elements having either the circular or rectangular aperture is given by

$$P^{NF}(R_{NF},\theta,\varphi,\theta_0,\varphi_0) = \sum_{p=1}^{m}\sum_{q=1}^{n} P_{pq}^{ENF}\left(R_{pq},\theta_{pq},\varphi_{pq}\right) \times A_{(p,q)}^{NF}\left(\theta_{pq},\varphi_{pq}\right) \times \ P_{(p,q)}^{NF}\left(\theta_{pq},\varphi_{pq}\right) \quad \text{(A.1)}$$

where,

$P^{NF}(R_{NF},\theta,\varphi,\theta_0,\varphi_0)$ is the radiation pattern of the beamforming array

$P_{pq}^{ENF}\left(R_{pq},\theta_{pq},\varphi_{pq}\right)$ is the radiation pattern of (p,q)th element

$A_{(p,q)}^{NF}\left(\theta_{pq},\varphi_{pq}\right)$ is array factor of (p,q)th element

$P_{(p,q)}^{NF}\left(\theta_{pq},\varphi_{pq}\right)$ is the beam steering phase of (p,q)th element

(R_{NF},θ,φ) denotes the Spherical coordinates of the observation point, P

(x_f, y_f, z_f) denotes the Cartesian coordinates of the observation point, P

$$x_f = R_{NF} \times sin\theta \times cos\varphi$$
$$y_f = R_{NF} \times sin\theta \times sin\varphi$$
$$z_f = R_{NF} \times cos\theta$$
$$-90^0 \leq \theta \leq +90^0 \quad ; \qquad 0^0 \leq \varphi \leq \quad 360^0$$

θ_0 and φ_0 are the desired angular coordinates of beam steering angles (elevation (θ_0) and azimuth (φ_0))

θ_{pq} is the elevation angle subtended by the (p,q)th element at the observation point

φ_{pq} is the azimuth angle subtended by the (p,q)th element at the observation point

The array factor $A^{NF}_{(q,p)}(\theta,\varphi)$ is given as

$$A^{NF}_{(p,q)}(\theta,\varphi) = e^{-jk(R_{pq}-R_{11})} \tag{A.2}$$

where,

$p = 1,2,3,\ldots.,m$

$q = 1,2,3,\ldots.,n$

m = Number of elements along x-axis

n = Number of elements along y-axis

R_{pq} = Distance between the (p,q)th array element and the observation point $P(x_f, y_f, z_f)$

R_{11} = Distance between the reference element (p=1,q=1) and the point of observation $P(x_f, y_f, z_f)$

$$x_{r_p} = x_1 + (p-1)dx$$
$$y_{r_q} = y_1 + (q-1)dy$$
$$Z_{r_{pq}} = 0$$

dx=inter-element spacing along x-axis
dy=inter-element spacing along y-axis
(x_1 y_1, z_1) denotes the Cartesian coordinates of the reference element of the array
x_1=0
y_1=0
z_1=0

$$R_{pq} = \sqrt{\left(x_f - x_{r_p}\right)^2 + \left(y_f - y_{r_q}\right)^2 + \left(z_f - z_{r_{pq}}\right)^2} \tag{A.3}$$

$$R_{11} = \sqrt{\left(x_f - x_1\right)^2 + \left(y_f - y_1\right)^2 + \left(z_f - z_1\right)^2} \tag{A.4}$$

$$\theta_{pq} = cos^{-1}\left(\frac{z_f - Z_{r_{pq}}}{R_{pq}}\right) \tag{A.5}$$

$$\varphi_{pq} = tan^{-1}\left(\frac{y_f - y_{rq}}{x_f - x_{rp}}\right) \tag{A.6}$$

The expression for the beam steering phase factor $P^{NF}_{(q,p)}(\theta_0, \varphi_0)$ in near field region at a given observation distance R_{NF} to steer the beam through an elevation angle θ_0 and azimuth angle φ_0 is given by

$$P^{NF}_{(p,q)}(\theta_0, \varphi_0) = e^{+jk(R_e - R_n)} \tag{A.7}$$

where,

R_e = Distance between the (p,q)th array element and the observation point $P(x_f, y_f, z_f)$ to steer the beam

$$x_{f_0} = R_{NF} \times sin\theta_0 \times cos\varphi_0$$
$$y_{f_0} = R_{NF} \times sin\theta_0 \times sin\varphi_0$$
$$z_{f_0} = R_{NF} \times cos\theta_0$$

$$R_e = \sqrt{\left(x_{f_0} - x_{r_p}\right)^2 + \left(y_{f_0} - y_{r_q}\right)^2 + \left(z_{f_0} - z_{r_{pq}}\right)^2} \tag{A.8}$$

$$R_n = \sqrt{\left(x_{f_0} - x_1\right)^2 + \left(y_{f_0} - y_1\right)^2 + \left(z_{f_0} - z_1\right)^2} \tag{A.9}$$

To compute the radiation pattern of an element of beamforming transducer array, $P^{ENF}_{pq}(R_{pq}, \theta_{pq}, \varphi_{pq})$, a generalized approach to determine the near-field radiation pattern of the acoustic transducer presented in (Praveen *et al.* 2021) can be followed. In this method, the acoustic aperture is assumed to comprise a number of point sources. The far-field radiation pattern of a point source is given by

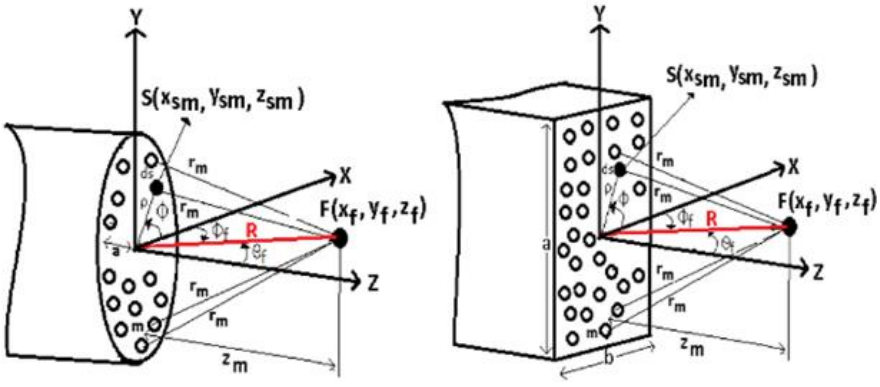

(a) Circular Aperture (b) Rectangular Aperture

Fig. A.2 Coordinate System of Circular and Rectangular Aperture for Near-Field Analysis

$$P_m(r_m) = A_m \frac{e^{-jkr_m}}{r_m} ds \tag{A.10}$$

Where "$P_m(r_m)$" is the corresponding amplitude of pressure of point source at a distance "r_m" from the source. The constant "A_m" defines the reference amplitude at the reference distance "r_m"; "km" is the wavenumber and j=√(-1); ds is infinitesimally small surface element of area. The pressure field distribution $P_f(x_f, y_f, z_f)$ at an observation point $F(x_f, y_f, z_f)$ due to the radiation from "m" point sources located at point $S\ (x_{sm}, y_{sm}, z_{sm})$ on circular aperture (Fig. A.2(a)) given in (Praveen *et al.* 2020) is

$$P_f^{ENF}(x_f, y_f, z_f) = \iint_{surface} P_m(x_{sm}, y_{sm}, z_{sm}) ds \tag{A.11}$$

$$P_f^{ENF}(x_f, y_f, z_f) = A_m \int_{\rho=0}^{a} \int_{\varphi=0}^{2\pi} \frac{e^{-jkr_m}}{r_m} \rho d\rho d\varphi \tag{A.12}$$

where,

A_m = Reference amplitude
k = Wave number
$j = \sqrt{(-1)}$
a= Radius of circular aperture
$0 \leq \rho \leq a \quad ; \quad 0 \leq \varphi \leq 2\pi$
r_m = Distance between m^{th} point source located on transducer aperture and observation point

The expression for computing radiation pattern of an acoustic transducer with a rectangular aperture (Fig. A.2(b)) given in (Praveen *et al.* 2020) is

$$P_f^{ENF}(x_f, y_f, z_f) = \iint_{surface} P_m(x_{sm}, y_{sm}, z_{sm}) ds \tag{A.13}$$

$$P_f^{ENF}(x_f, y_f, z_f) = A_m \int_{-W/2}^{W/2} \int_{-L/2}^{:L/2} \frac{e^{-jkr_m}}{r_m} dx dy \tag{A.14}$$

where,

r_m = Distance between m^{th} point source located on transducer aperture and observation point
L = Length of the rectangular aperture
W= Width of the rectangular aperture

The flowchart for the implementation of UAI system in MATLAB environment is shown in Fig. A.3.

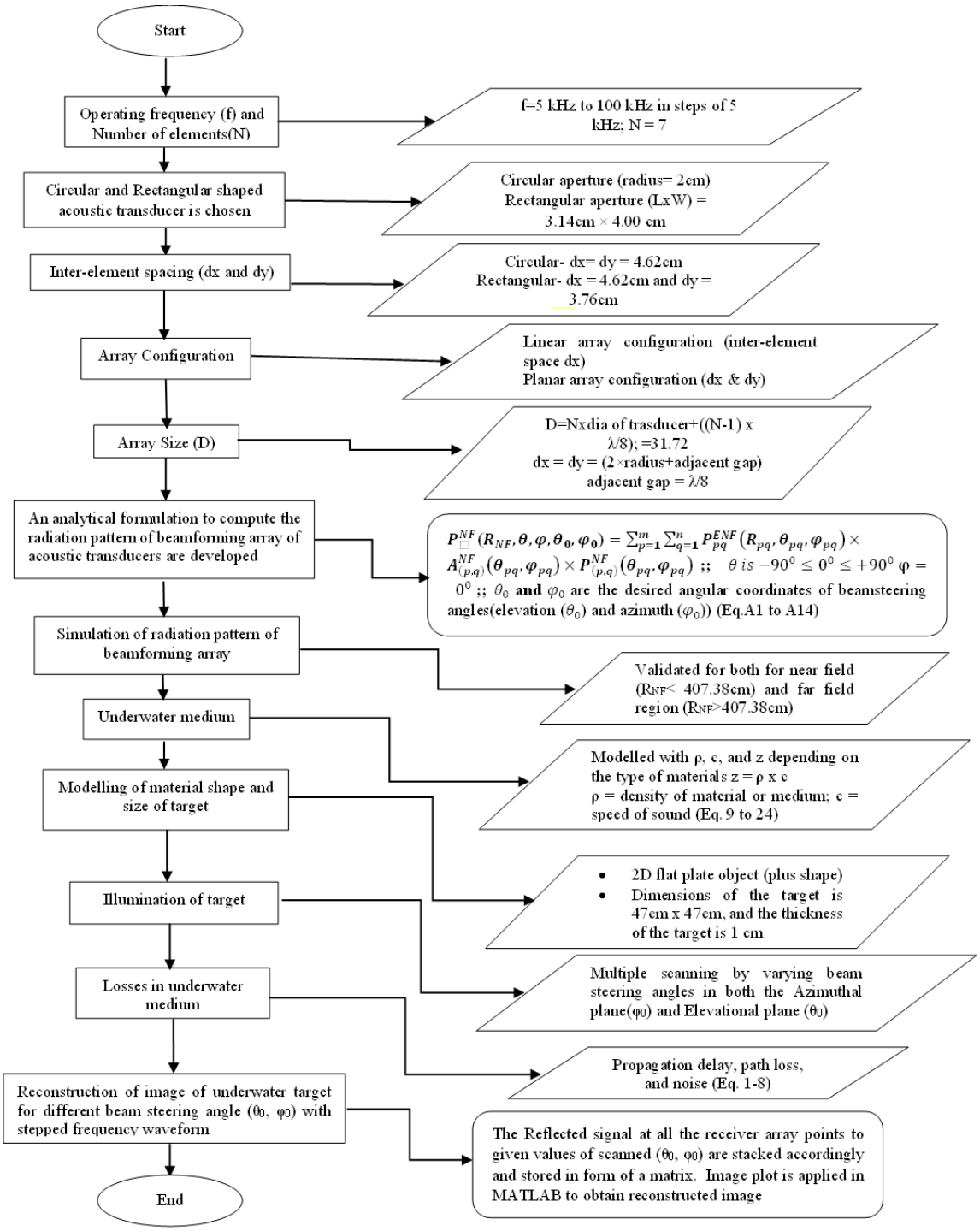

Fig. A.3 Implementation of Simulation Model for UAI system in MATLAB Environment